Influences of the mixed LiCl-$CaCl_2$ liquid desiccant solution on a membrane-based dehumidification system: parametric analysis and mixing ratio selection

Hongyu Bai[a], Jie Zhu[a,*], Junze Chu[a], Xiangjie Chen[a], Yuanlong Cui[a], Yuying Yan[a,b]

[a] *Department of Architecture and Built Environment, the University of Nottingham, University Park, Nottingham, United Kingdom*

[b] *Centre for Fluids & Thermal Engineering, University of Nottingham, Ningbo, China*

Abstract

The membrane-based liquid desiccant dehumidification system has high energy efficiency without the traditional liquid system carry-over problem. The performance of such a system strongly depends on solution's temperature and concentration, which have direct relationship to the solution surface vapour pressure. Compared with the pure liquid desiccant solution, the mixed liquid desiccant solution has lower surface vapour pressure, better system performance and lower material cost. In this paper, the performance of a flat-plate membrane-based liquid desiccant dehumidification system with the mixed solution (LiCl and $CaCl_2$) is investigated through theoretical and experimental approaches. A mathematical model is established to predict the system performance, while the electrolyte non-random two-liquid (NRTL) method is applied to calculate the mixed solution properties. The influences of the solution mixing ratio, temperature T_{sol} and concentration C_{sol} are evaluated, and it is found that the regeneration heat Q_{reg} can be dramatically reduced by either applying a high concentration solution or increasing $CaCl_2$ content in the mixed solution. Compared with the pure LiCl solution system, the mixed solution system COP can be improved up to 30.23% by increasing $CaCl_2$ content for a 30% concentration solution. The optimum mixing ratio varies with the solution concentration. For the mixed LiCl-$CaCl_2$ solution, the system highest COPs appear at the mixing ratios of 3:1, 2:1 and 1:1 for 20%, 30% and 40% concentrations respectively.

Keywords: dehumidifier, membrane, COP, mixed solution

* *Corresponding author: jie.zhu@nottingham.ac.uk (J.Zhu).*

1. Introduction

Indoor thermal comfort and good air quality are two of the most important factors which a building should provide for its occupants. Heating, ventilation and air-conditioning (HVAC) system plays a crucial role in providing healthy and comfort environment [1-3], which consumes more than 50% of the building total energy. In fact, approximately 20-40% of the energy consumed by HVAC system is used for air dehumidification. The traditional mechanical vapour compression dehumidification approach has several problems, such as the growths of mould and bacteria on the wet surfaces, and additional energy used for air re-heating, which result in the poor indoor air quality and huge energy consumption [4-8].

In recent years, the extensive researches have been conducted on liquid desiccant cooling system owing to its advantages: better ability to deal with the latent heat load, more energy efficient and healthily friendly compared with the traditional system [9-11]. In such a system, the liquid desiccant solution is used to absorb moisture from the supply air directly to achieve dehumidification function. The packed beds are traditionally used as heat and mass transfer contractors, in which the liquid desiccant and air are in direct contact. As a result, the small corrosive desiccant droplets are carried over and supplied to the conditioned space, which brings concern to the indoor environment and occupants' health [12-14]. Selectively permeable membranes have been used in the liquid desiccant dehumidification systems as an alternative to the packed beds to overcome the carry-over problem [12], and the desiccant solution and air channels are separated by the membranes to prevent the solution from crossing over to the air flow.

The extensive studies have focused on the membrane-based dehumidification system recently. Zhang at al. [15-18] investigated heat and mass transfer mechanism in both air-to-air and solution-to-air cross-flow membrane based enthalpy exchanger under real boundary condition. Then they calculated local and mean Nusselt and Sherwood numbers by solving the coupled governing equations directly. Moghaddam et al. [19-21] assessed the operating characteristics of a liquid-to-air membrane energy exchanger (LAMEE), and evaluated the influences of thermal capacity ratio (Cr^*), heat transfer unit (NTU) and operating condition. They found NTU to be the most crucial parameter affecting the system effectiveness. Vali et al. [22] studied a counter-cross LAMEE by investigating the effects of aspect and entrance ratios through numerical modelling, and discovered that the counter-cross-flow configuration would have the same performance as the counter-flow configuration if the membrane surface area is enlarged by 10%. Moghaddam et al. [23] introduced a solution-side effectiveness to evaluate the impact of Cr^* on dehumidification and regeneration processes, and pointed out that the latent effectiveness difference between the air-side and the solution-side is can be neglected. Bai et al. [24, 25] experimentally and theoretically studied the operating characters of a parallel-plate

membrane-based dehumidification system by focusing on various parameters, and identified the effects of NTU and mass flow rate ratio (m^*) are interacted with each other. Some researchers developed different types of the membrane-based contractor. Dong et al. [26] found that by applying TiO_2 super hydraulic coating for a dehumidifier would significantly improve its performance and save building energy consumption. Liu et al. [27] made a detailed quantitative comparison of three novel internally-cooled dehumidifiers and discovered that the most important reason for performance difference is mass transfer ability. Qiu et al. [28] investigated laminar flow and heat transfer in an internally-cooled hexagonal parallel-plate membrane channel (IHPMC), then obtained the mean Reynold and Nusselt numbers. Huang et al. [29-31] investigated the performance of an internally-cooled membrane-based contractor and found that its performance is much better than the adiabatic one's, and can be largely improved by decreasing water inlet temperature. Lin et al. [32] studied a hybrid membrane-based dehumidification system combined with dew point evaporative cooling technology, and discovered such a hybrid system is capable of meeting the humidity (less than 12.0 g/kg) and temperature (between 19.5 and 28 ℃) requirements for most simulated conditions.

The properties of liquid desiccant are closely related to its vapour pressure, as a result the system effectiveness varies significantly with the liquid desiccant. The working fluids in the above mentioned researches are either pure LiCl or pure $CaCl_2$ solution. LiCl is the most stable liquid desiccant but with high cost, while $CaCl_2$ is the cheapest and most readily available liquid desiccant but with relatively unstable state. Compared with the single desiccant solution, some mixed desiccant solutions have the better dehumidification efficiency, lower material cost and energy consumption [33]. Ertas et al. [34] experimentally tested the properties of the mixed LiCl-$CaCl_2$ desiccant solution under 20% of mass concentration, and proposed a mixing ratio of 1:1 for the best performance. Ahmed et al. [35] predicted the vapour pressure of the mixed LiCl-$CaCl_2$ desiccant solution using a simple mixing rule (SMR) proposed by Nilson [36]. However the SMR is not capable of calculating the properties of the mixed desiccant solution accurately. Then Chen and Evans [37] and Chen et al. [38] proposed an electrolyte non-random two-liquid (NRTL) method which uses only binary parameters. Yao et al. [39] compared these two methods by testing the surface vapour pressure of the mixed solution under different circumstances, and found that the SMR shows the better accuracy when the mixed solution concentration is below 10%, while the NRTL method is much more accurate when the solution concentration is higher than 30%. Zhu and Yao [40] investigated the optimum mixing ratio of LiCl-$CaCl_2$ solution to be 1:1 by NRTL method and are verified through measuring the vapour pressures of various mixture ratios and mass concentrations of mixed solution under different temperatures. Zhao et al. [33] and Li et al. [41, 42] applied the NRTL method to investigate the optimal ratio of the mixed LiCl-$CaCl_2$ desiccant solution for a direct contact liquid desiccant dehumidification system. Nevertheless, there are few studies on the influences of different

mixing ratios and the optimum mixing ratio for the membrane-based liquid desiccant dehumidification system. The objective of this paper is to investigate the effects of the mixed LiCl-$CaCl_2$ desiccant solution properties (i.e. temperature T_{sol}, concentration C_{sol} and mixing ratio of LiCl and $CaCl_2$) on the performance of a membrane-based liquid desiccant dehumidification system by numerical modelling and experimental tests. The optimum mixing ratio of the LiCl-$CaCl_2$ desiccant is determined based on dehumidification capacity and COP analyses. By comparing with the experimental results, this paper comes out a method to predict the system performance with the mixed solution by combining the NRTL method and numerical modelling. It presents a comprehensive investigation on the effects of the mixed LiCl-$CaCl_2$ desiccant properties on the membrane-based liquid desiccant dehumidification system, and provides an approach for the optimum mixing ratio selection through the system performance and COP analyses.

2. Mixed desiccant properties

The predictions of the mixed desiccant properties (such as surface vapour pressure and specific humidity ratio) under different mixing ratios, temperatures and concentrations are of vital importance. As presented in the introduction section, the SMR method is only capable of predicting the mixed desiccant properties when its concentration is lower than 10%. By contrast, the NRTL method provides more accurate calculation for the mixed desiccant solution with over 30% concentration. The NRTL method uses only binary parameters to correlate and predict the deviation from ideality of aqueous multi-component electrolyte system over the entire ranges of temperature and concentration [39]. Thus the NRTL method is adopted in this study to calculate the mixed desiccant surface vapour pressure.

The vapour-liquid equilibrium relation for water in an electrolyte solution can be given as [37]:

$$a_w = \frac{P_{v,sol}}{P_{v,w}} \tag{1}$$

$$a_w = x_w f_w \tag{2}$$

Where a_w is activity of water; $P_{v,sol}$ and $P_{v,w}$ are vapour pressures of the solution and water respectively (Pa); x_w is mole concentration of water; f_w is activity coefficient of water.

The vapour pressure of water can be obtained by using August-Roche-Magnus equation [43]:

$$P_{v,w} = 0.61094 exp\left(\frac{17.625T}{T+243.04}\right) \tag{3}$$

Where $P_{v,w}$ is water vapour pressure (kPa); T is water temperature (℃).

The solution vapour pressure can be obtained once the activity of water is determined, which is the product of water mole concentration x_w and activity coefficient f_w. The calculation of f_w can be divided into two parts: long-range and short-range interaction contributions, as can be expressed as [37]:

$$lnf_w = lnf_w^{LRC} + lnf_w^{SRC} \tag{4}$$

The long-range interaction contribution f_w^{LRC} can be calculated by using Pitzer-Debye-Huckel function:

$$ln f_w^{LRC} = \left(\frac{1000}{M_w}\right)\frac{2A_\phi I_x^{3/2}}{1+\chi I_x^{1/2}} \quad (5)$$

Where M_w is molecular weight of water, which is 0.018 kg/mol; A_ϕ is Debye-Huckel constant for the osmotic coefficient, which is 0.391; I_x is ionic strength in mole fraction, which equals $0.5\sum x_i z_i^2$, where x_i is mole fraction of any species in the mixed desiccant solution, and z_i is corresponding absolute value of ionic charge ; χ is the closest approach parameter of the Pitzer-Debye-Huckel equation, which is 14.9.

For the LiCl-$CaCl_2$ desiccant, Eq. (5) can be derived to [37]:

$$ln f_w^{LRC} = 5.829 \times \frac{x_{LiCl}+3x_{CaCl_2}}{1+14.9(x_{LiCl}+3x_{CaCl_2})^{1/2}} \quad (6)$$

The short-range interaction in LiCl-$CaCl_2$ electrolyte can be expressed as:

$$ln f_w^{SRC} = (-x_w)\frac{2A\tau_{LiCl,w}x_{LiCl}+4B\tau_{CaCl_2,w}x_{CaCl_2}}{\left(2Ax_{LiCl}+4Bx_{CaCl_2}+x_w\right)^2} + \frac{2A\tau_{LiCl,w}x_{LiCl}+4B\tau_{CaCl_2,w}x_{CaCl_2}}{1+(2A-2)x_{LiCl}+(4B-3)x_{CaCl_2}} +$$

$$(x_{LiCl}A') \times \frac{\tau_{w,LiCl}x_{LiCl}+2\left[C'(\tau_{w,LiCl}-\tau_{CaCl_2,LiCl})+2\tau_{w,LiCl}\right]x_{CaCl_2}}{\left[(1-2A')x_{LiCl}+(2C'+2-3A')x_{CaCl_2}+A'\right]} + \left(2B'x_{CaCl_2}\right) \times$$

$$\frac{\left[C(\tau_{w,CaCl_2}-\tau_{LiCl,CaCl_2})+\tau_{w,CaCl_2}\right]x_{LiCl}+2\tau_{w,CaCl_2}x_{CaCl_2}}{\left[(C+1-2B')x_{LiCl}+(2-3B')x_{CaCl_2}+B'\right]^2} + (x_{LiCl}A') \times$$

$$\frac{\tau_{w,LiCl}x_{LiCl}+2C'(\tau_{w,LiCl}-\tau_{CaCl_2,LiCl})x_{CaCl_2}}{\left(x_{LiCl}+2C'x_{CaCl_2}+A'x_w\right)^2} + (2B'x_{CaCl_2}) \times$$

$$\frac{C(\tau_{w,CaCl_2}-\tau_{LiCl,CaCl_2})x_{LiCl}+2\tau_{w,CaCl_2}x_{CaCl_2}}{(Cx_{LiCl}+2x_{CaCl_2}+B'x_w)^2} \quad (7)$$

Where A, B, C, A', B' and C' represent:

$A = e^{(-0.2\tau_{LiCl,w})}$

$B = e^{(-0.2\tau_{CaCl_2,w})}$

$C = e^{(-0.2\tau_{LiCl,CaCl_2})}$

$A' = e^{(-0.2\tau_{w,LiCl})}$

$B' = e^{(-0.2\tau_{w,CaCl_2})}$

$C' = e^{(-0.2\tau_{CaCl_2,LiCl})}$

Where $\tau_{LiCl,w}$, $\tau_{CaCl_2,w}$, $\tau_{w,LiCl}$, $\tau_{w,CaCl_2}$, $\tau_{LiCl,CaCl_2}$ and $\tau_{CaCl_2,LiCl}$ are binary interaction energy parameters, which are given at 25℃ and listed in Table 1.

Table 1

Parameters of binary interaction energy for mixed solution activity coefficient calculation (25℃)

parameter	$\tau_{LiCl,w}$	$\tau_{CaCl_2,w}$	$\tau_{w,LiCl}$	$\tau_{w,CaCl_2}$	$\tau_{LiCl,CaCl_2}$	$\tau_{CaCl_2,LiCl}$
value	-5.1737	-5.2549	10.1242	10.5126	0	0

For the binary interaction energy parameters at different temperatures, the following correlation should be applied [37]:

$$\tau_{(T)} = \frac{298.15}{T+273.15}\tau_{(25℃)} \quad (8)$$

Where $\tau_{(25℃)}$ is binary interaction energy parameter at 25℃ as given in Table 1.

In Eq. (7), x_{LiCl} and x_{CaCl_2} are mole concentrations of LiCl and $CaCl_2$ respectively, and there exits such a relationship:

$$x_{LiCl} + x_{CaCl_2} + x_w = 1 \quad (9)$$

Then the mixed solution vapour pressure $P_{v,sol}$ can be obtained by solving Eqs. (1) - (9). Once $P_{v,sol}$ is obtained, the solution specific humidity ratio W_{sol} $(kg/kg\ \ dry\ air)$ can be calculated by [44]:

$$W_{sol} = 0.62198\frac{P_{v,sol}}{P-P_{v,sol}} \quad (10)$$

Where P is atmospheric pressure (Pa).

3. Numerical modelling

3.1 Governing equations

Once the mixed desiccant solution properties are obtained, the numerical model for a membrane-based parallel-plate dehumidifier can be developed. The schematics of the dehumidifier and coordinate system applied for numerical model are given in Fig. 1. The solution and air flows are separated by the flat-plate membranes, and they are in a cross-flow configuration. As seen in Fig. 1 that the calculating domain consists of one solution channel, its adjacent air channel and the middle membrane.

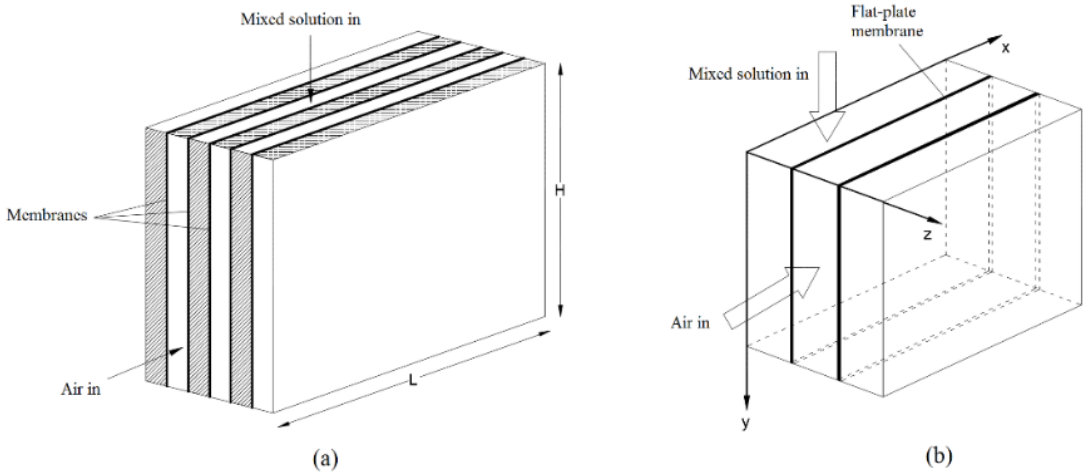

Fig. 1. Schematics of cross flow parallel-plate dehumidifier and regenerator (a), and coordinate system applied for numerical simulation (b).

The assumptions made for numerical modelling are given as:

- The dehumidifier is well-insulated and there is no heat transfer with its surrounding environment.
- The flows in both the air and solution channels are assumed to be fully-developed laminar flows, and the changes of their temperatures, humidity ratios or concentrations are along the channel length.
- The directions of heat and mass flows are normal to the membrane surface.
- The heat generated during the water vapour adsorption is released to the solution channel only.

Afterwards, the normalized governing equations of heat and moisture exchanges for the solution and air sides can be established as:

Solution side:

$$\frac{\partial {T_{sol}}^*}{\partial y^*} - NTU_m h^* \frac{1}{Cr^*}\left({W_{air}}^* - {W_{sol,mem}}^*\right) - NTU \frac{1}{Cr^*}({T_{air}}^* - {T_{sol}}^*) = 0 \quad (11)$$

$$\frac{\partial X_{sol}}{\partial y^*} - NTU_m \frac{1}{m^*} W_0 (1 + X_{sol})({W_{air}}^* - {W_{sol,mem}}^*) = 0 \quad (12)$$

Air side:

$$\frac{\partial {T_{air}}^*}{\partial x^*} + NTU({T_{air}}^* - {T_{sol}}^*) = 0 \quad (13)$$

$$\frac{\partial {W_{air}}^*}{\partial x^*} + NTU_m\left({W_{air}}^* - {W_{sol,mem}}^*\right) = 0 \quad (14)$$

Where X_{sol} is solution mass fraction, and calculated by:

$$X_{sol} = \frac{\dot{m}_{water}}{\dot{m}_{desi}} = \frac{1 - C_{sol}}{C_{sol}} \quad (15)$$

Where C_{sol} is solution mass concentration:

$$C_{sol} = \frac{\dot{m}_{desi}}{\dot{m}_{sol}} \quad (16)$$

Where $\dot{m}_{desi}$ and $\dot{m}_{sol}$ are liquid desiccant and solution mass flow rates respectively (kg/s). In the above governing equations, the dimensionless properties are adopted. $x^*$is dimensionless length given by:

$$x^* = \frac{x}{L} \tag{17}$$

y^* is dimensionless height given by:

$$y^* = \frac{y}{H} \tag{18}$$

Where L and H are length and height of the dehumidifier unit respectively (m).

T^* is dimensionless temperature given by:

$$T^* = \frac{T - T_{air,in}}{T_0} \tag{19}$$

Where $T_{air,in}$ is air inlet temperature (℃); T_0 is equal to $(T_{sol,in} - T_{air,in})$, $T_{sol,in}$ is solution inlet temperature (℃).

W^* is dimensionless humidity ratio given by:

$$W^* = \frac{W - W_{air,in}}{W_0} \tag{20}$$

Where $W_{air,in}$ is air inlet humidity ratio (kg/kg); W_0 is equal to $(W_{sol,in} - W_{air,in})$; $W_{sol,in}$ is solution inlet humidity ratio (kg/kg).

$m^*$is mass flow rate ratio given as follows:

$$m^* = \frac{\dot{m}_{sol}}{\dot{m}_{air}} \tag{21}$$

Where $\dot{m}_{air}$ is air mass flow rate (kg/s).

Cr^* is thermal capacity ratio and defined by:

$$Cr^* = \frac{(\dot{m}c_p)_{sol}}{(\dot{m}c_p)_{air}} \tag{22}$$

$c_{p,sol}$ and $c_{p,air}$ are specific heat capacities at constant pressure of the solution and air respectively (kJ/kgK).

$h^*$is operating factor and given as:

$$h^* = \frac{W_0}{T_0}\frac{h_{fg}}{c_{p,air}} \tag{23}$$

Where h_{fg} is phase change heat of water during water vapour adsorption (J/kg).

NTU and NTU_m are defined as the numbers of heat and mass transfer respectively, and can be obtained:

$$NTU = \frac{UA}{(\dot{m}c_p)_{air}} \tag{24}$$

$$NTU_m = \frac{U_m A}{\dot{m}_{air}} \tag{25}$$

Where A is total membrane surface area (m^2). U (W/m^2K) and U_m (kg/m^2s) are heat and mass transfer coefficients respectively, and can be obtained by:

$$U = \left(\frac{1}{h_{air}} + \frac{\delta}{k_{mem}} + \frac{1}{h_{sol}}\right)^{-1} \quad (26)$$

$$U_m = \left(\frac{1}{h_{m,air}} + \frac{\delta}{k_{m,mem}}\right)^{-1} \quad (27)$$

Where h_{air} and h_{sol} are convective heat transfer coefficients in the air and solution sides respectively (W/m^2K); $h_{m,air}$ is mass transfer coefficient (kg/m^2s) in the air side; δ is the thickness of membrane(m); k_{mem} (W/mK) and $k_{m,mem}(kg/ms)$ are membrane heat and mass transfer conductivity respectively.

3.2 Boundary conditions

The boundary conditions for the numerical model are given as:

Solution side:

${T_{sol}}^* = 1$, at y^*=0 (28)

$X_{sol} = X_{sol,in}$, at y^*=0 (29)

Air side:

${T_{air}}^* = 0$, at x^*=0 (30)

${W_{\text{air}}}^* = 0$, at x^*=0 (31)

To solve Eqs. (11) – (14), another two equations based on the conservations of heat and mass flows through the membrane should be established as follows:

$$NTU_{sol}\left({T_{sol,mem}}^* - {T_{sol}}^*\right) = NTU\left({T_{air}}^* - {T_{sol,mem}}^*\right) + NTU_m h^*\left({W_{air}}^* - {W_{sol,mem}}^*\right) \quad (32)$$

$$NTU_m W_0\left({W_{air}}^* - {W_{sol,mem}}^*\right) = NTU_{m.sol}(C_{sol} - C_{sol,mem}) \quad (33)$$

Where $C_{sol,mem}$ is the mass concentration of liquid desiccant on the membrane surface; NTU_{sol} is number of heat transfer unit in the solution side and can be calculated by:

$$NTU_{sol} = \frac{h_{sol}A}{(\dot{m}c_p)_{air}} \quad (34)$$

$NTU_{m.sol}$ is number of mass transfer unit in the solution side, and defined by:

$$NTU_{m.sol} = \frac{h_{m,sol}A}{\dot{m}_{air}} \quad (35)$$

Where $h_{m,sol}$ is mass transfer coefficient in the solution side (kg/m^2s).

3.3 Simulation procedure

The finite difference method is applied to solve the governing equations, which are discretized by using the forward difference scheme.

The coupled governing equations for air and solution flows are solved in the Matlab. The numerical tests are carried out to decide the proper grid size, and it is found that 30×60 grids are sufficient in current study. The result difference is less than 1.0% compared with 50×100 grid's, so the numerical uncertainty is 1.0%. The flow chart of the calculating method used for numerical modelling is demonstrated in Fig. 2.

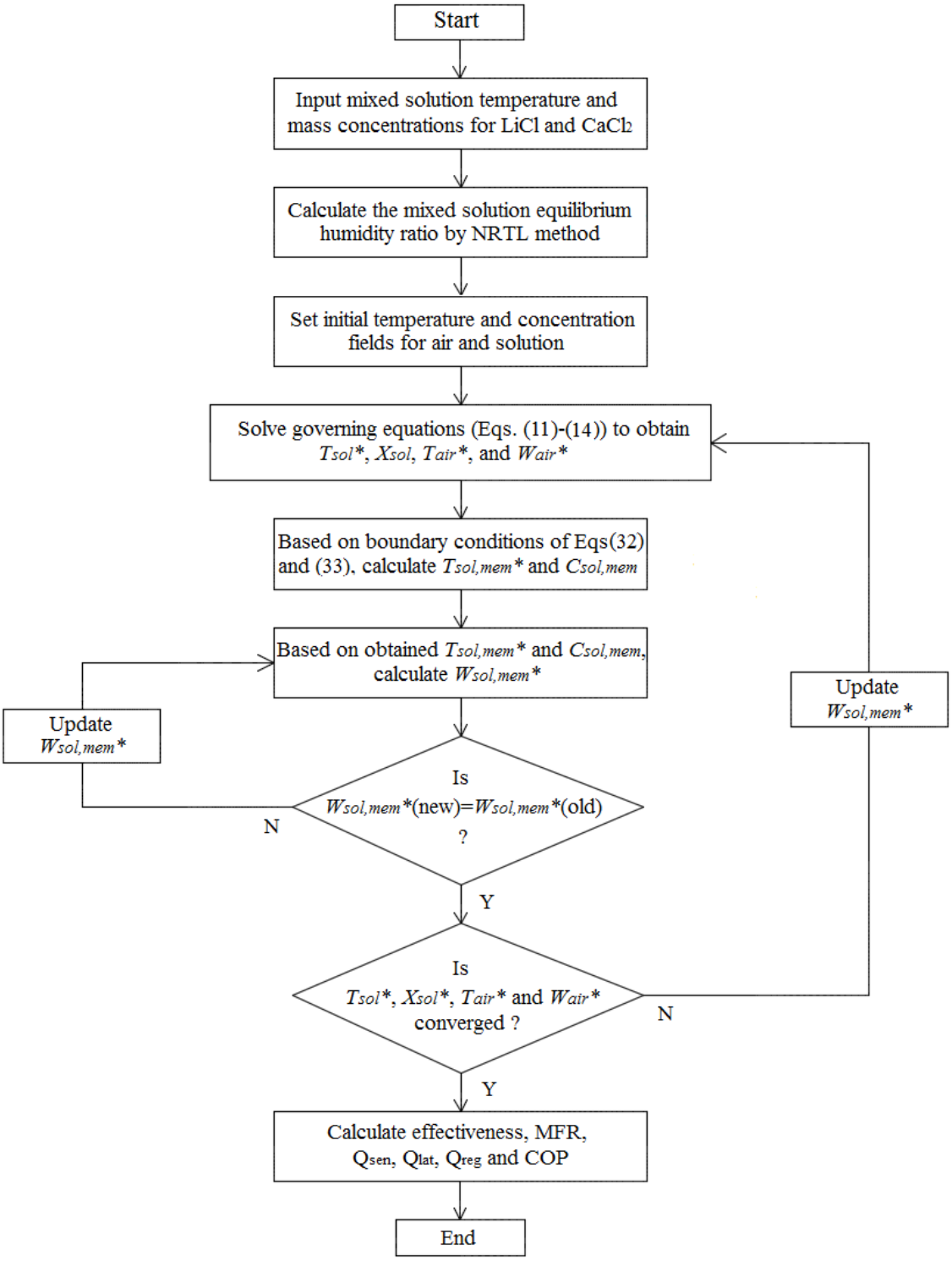

Fig. 2. Flow chart of the calculating method used for numerical modelling

4. System performance indexes

4.1. Effectiveness of dehumidifier

The effectiveness is a critical index applied for the performance evaluation of a heat and mass exchanger. The most important functions of the dehumidifier are to absorb air moisture and reduce its temperature as well. Thus in this study, two types of the effectiveness referring the

air side in the dehumidifier are defined: sensible effectiveness (ε_{sen}) and latent effectiveness (ε_{lat}). ε_{sen} is the ratio between the actual sensible heat transfer and the maximum potential amount of sensible heat transfer. ε_{lat} is the ratio between the actual amount of moisture transferred and the maximum possible amount of moisture transferred in a mass exchanger. When $Cr^* \geq 1$, meaning the desiccant solution thermal capacity is higher than that of air, the sensible and latent effectiveness can be defined by Eqs. (36) and (37) [45].

$$\varepsilon_{sen} = \frac{T_{air,in} - T_{air,out}}{T_{air,in} - T_{sol,in}} \tag{36}$$

$$\varepsilon_{lat} = \frac{W_{air,in} - W_{air,out}}{W_{air,in} - W_{sol,in}} \tag{37}$$

Where $T_{air,out}$ is air outlet temperature (℃), and $W_{air,out}$ is air outlet humidity ratio (kg/kg).

4.2. Moisture flux rate

The moisture removal rate (MRR) is an evaluation of the quantity of moisture absorbed by dry air from the weak liquid desiccant during regeneration, or the quantity of moisture in moist air absorbed by the strong liquid desiccant during dehumidification. For the dehumidifier, it is expressed as:

$$MRR = \dot{m}_{air}\left(W_{air,in} - W_{air,out}\right) \tag{38}$$

Afterward, the moisture flux rate (MFR) is presented:

$$MFR = \frac{MRR}{U_m A} = \frac{\dot{m}_{air}\left(W_{air,in} - W_{air,out}\right)}{U_m A} \tag{39}$$

It can be seen from Eq. (39) that the MFR is the ratio of moisture removal rate MRR over the membrane overall mass transfer conductance. In this study the MFR is used for performance analysis rather than the MFF since compared with the MRR, the MFR is independent of the dehumidifier size and it is only related to inlet state.

4.3. Coefficient of performance (COP)

The COP of the membrane-based liquid desiccant dehumidification system can be defined as:

$$COP = \frac{Q_{sen} + Q_{lat}}{Q_{reg}} \tag{40}$$

Where Q_{sen}, Q_{lat} and Q_{reg} are sensible cooling output, latent cooling output and regeneration power input (kW) respectively, which can be calculated by:

$$Q_{sen} = \dot{m}_{air} c_{p,air} (T_{air,in} - T_{air,out}) \tag{41}$$

$$Q_{lat} = MRR \times h_{fg} = \dot{m}_{air} h_{fg} \left(W_{air,in} - W_{air,out}\right) \tag{42}$$

$$Q_{reg} = \dot{m}_{sol} c_{p,sol} (T_{reg} - T_{sol,out}) \tag{43}$$

Where $T_{sol,out}$ is solution temperature at the dehumidifier outlet (℃), T_{reg} is required solution temperature at the regenerator inlet (℃).

5. Experimental tests

A liquid desiccant dehumidification test rig has been built in the Marmont Lab of University of Nottingham, which is illustrated in Fig. 3.

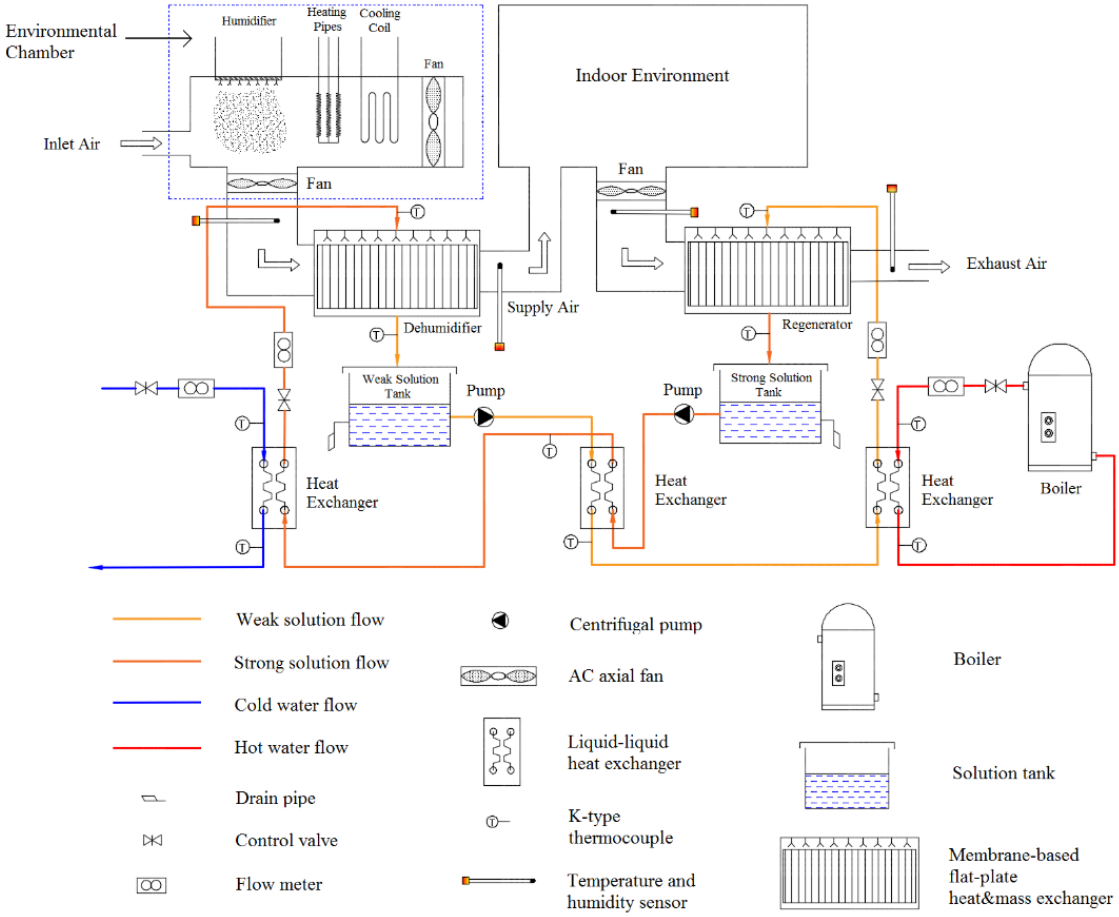

Fig. 3. Schematic diagram of the experimental testing rig

The main components of the membrane-based dehumidification system include one dehumidifier, one regenerator, two storage tanks and three liquid-liquid heat exchangers. An environmental chamber as shown in dashed blue line frame in Fig. 3 equipped with several cooling coils, heating pipes and a humidifier is used in the rig to provide the high humidity and temperature supply air for the dehumidifier. Through the dehumidifier, both the humidity ratio and temperature of the supply air are reduced by the cold desiccant solution, then the air is supplied to the indoor environment. The exhaust air from the indoor environment is used for the desiccant solution regeneration. In the regenerator, the air is heated and humidified by the diluted solution with high temperature. Eventually it is discharged to the outside. The air flow rates for the dehumidifier and regenerator are adjusted by two AC axial fan rotation speeds. The dehumidifier is 410mm in length, 230mm in width and 210mm in height, has eleven air flow channels and eleven solution flow channels. The dehumidifier dimensions and the membrane physical properties are given in Table 2.

Table 2

Dehumidifier dimensions and membrane physical properties.

Description	Notation	Unit	Number
Length of dehumidifier	L	m	0.41
Width of dehumidifier	W	m	0.23
Height of dehumidifier	H	m	0.21
Air channel thickness	d_{air}	m	0.0077
Solution channel thickness	d_{sol}	m	0.0043
Membrane thickness	δ_{mem}	m	0.5×10^{-3}
Membrane conductivity	k_{mem}	kW/mK	3×10^{-4}
Membrane mass transfer conductivity	$k_{m,mem}$	kg/ms	3.87×10^{-6}

To make the mixed solution with the specific mixing ratio and concentration, firstly the mixing ratio is achieved at a low concentration, then more LiCl and $CaCl_2$ are added to the mixed solution to increase its concentration. For example, to make a 1:1 mixed solution, the same amounts of LiCl and $CaCl_2$ are added into water to make a 30% mixed solution. Then the water remains unchanged, more LiCl and $CaCl_2$ with the same amount are added into the solution to increase its concentration (e.g. 36% and 39%). This procedure is also used for the other mixing ratios. The solution circulation is achieved by two 15W centrifugal magnetically driven pumps, and their flow rates in the dehumidifier and regenerator are measured by two liquid flow indicators. The concentrated solution is cooled by cold water before entering the dehumidifier. The diluted solution is collected by the weak solution tank and then pumped into the regenerator through a heat exchanger, its temperature is increased in the heat exchanger by hot water provided by an electrical boiler with temperature range of 20℃ to 80℃, and its flow rate is measured by another liquid flow indicator. The air inlets and outlets in the dehumidifier and regenerator are installed with temperature and humidity sensors. Thermocouples are installed at inlets and outlets of water and desiccant flows to measure their temperatures. All sensors are linked to a data recorder for data collection and all data are eventually sent to the computer. The dehumidifier, regenerator, heat exchangers, solution tanks, water and solution pipes are properly insulated to minimize the environmental impact. All devices and their corresponding accuracies are shown in Table 3. Uncertainty analysis is carried out by applying the propagation method [46] to calculate uncertainties for the experimental data. According to [46] for the uncertainty in sums and differences, or in products and quotients, the uncertainty in the computed value of q can be calculated by:

$$Sums\ and\ differences\text{:}\ \ \delta q \approx \sqrt{(\delta x)^2 + \cdots + (\delta z)^2} \tag{44}$$

$$Products\ and\ quotients\text{:}\ \frac{\delta q}{|q|} \approx \sqrt{\left(\frac{\delta x}{|x|}\right)^2 + \cdots + \left(\frac{\delta z}{|z|}\right)^2} \tag{45}$$

Where $x, \cdots, z$ are measured quantities.

If q is any function of several variables $x, \cdots, z$, the uncertainty of q can be obtained by:

$$\delta q = \sqrt{\left(\frac{\partial q}{\partial x}\delta x\right)^2 + \cdots + \left(\frac{\partial q}{\partial z}\delta z\right)^2} \quad (46)$$

By applying Eqs (44)-(46), the absolute uncertainties of calculated values can be obtained. Error bars are included in all experimental data.

Table 3

Devices used for measurement and their uncertainties.

Measurement equipment	Parameter	Range	Uncertainty
Testo thermos-anemometer	Air speed	0-10 m/s	$\pm 5\%$
Sensiron Evaluation KIT EK-H4	Temperature	-40-125 ℃	$\pm 0.4\%$
	Relative humidity	0-100 %	$\pm 3\%$
K-type thermocouple probe	Temperature	0-1100 ℃	$\pm 0.75\%$
DT500 Data recorder	Data collection	-	$\pm 0.15\%$
Parker UCC PET flow indicator	Solution flow rate	1-15 L/min	$\pm 5\%$
Parker FM 26 122 212 flow indicator	Water flow rate	2-22 L/min	$\pm 5\%$

6. Model validation

The numerical model and NRTL method are validated by experimental data. The experiment process consists of two stages, and total 28 tests under different designed operating conditions have been completed in this study. At first, 15 tests are carried out to verify the sensible and latent effectiveness. The operating conditions, together with numerically obtained and experimentally collected values of the effectiveness are given in Table 4. Another 13 tests are conducted in the second stage to validate the moisture flux rate. The solution and air mass flow rates are kept constant through all the tests for the same m^* and NTU. The moisture flux rate comparisons between the numerical calculations and the experimental data are given in Table 5.

It can be seen in Table 4 that the simulation results of ε_{sen} and ε_{lat} generally are in accordance with the measurement data. The maximum discrepancies for ε_{sen} and ε_{lat} are 3.679% and 6.257% respectively. The maximum difference for the MFR is 15.510% as indicated in Table 5. As seen, generally the numerical model predicts the heat and moisture transfer in the dehumidifier well. The numerical modelling results are in good agreement with experimental data, and they have similar variation trends. This means the developed numerical model with the NRTL method predicts the system performance accurately and can predict the characteristics of this system rather successfully.

Table 4

Sensible and latent effectiveness under various designed operating conditions, comparison of numerical and experimental results

Designed operating conditions						Comparisons					
$T_{sol,in}$ (℃)	$C_{sol,in}$ (%)	X_{LiCl}	X_{CaCl2}	m_{air} (kg/s)	m_{sol} (kg/s)	$\varepsilon_{sen,num}$	$\varepsilon_{sen,exp}$	Error (%)	$\varepsilon_{lat,num}$	$\varepsilon_{lat,exp}$	Error (%)
16	30	1	0	0.0495	0.099	0.8604	0.838	2.603	0.7012	0.687	2.025
16	30	2	1	0.0495	0.099	0.8555	0.825	3.565	0.7486	0.714	4.622
16	30	1	1	0.0495	0.099	0.8530	0.832	2.462	0.7807	0.739	5.341
16	30	1	2	0.0495	0.099	0.8504	0.829	2.516	0.8216	0.803	2.264
16	30	0	1	0.0495	0.099	0.8448	0.815	3.527	0.9454	0.894	5.437
16	36	1	0	0.0495	0.099	0.8479	0.818	3.526	0.7658	0.732	0.414
16	36	2	1	0.0495	0.099	0.8427	0.813	3.524	0.8046	0.785	2.436
16	36	1	1	0.0495	0.099	0.8399	0.809	3.679	0.8311	0.796	4.223
16	36	1	2	0.0495	0.099	0.8371	0.807	3.596	0.8658	0.818	5.521
16	36	0	1	0.0495	0.099	0.8310	0.808	2.768	0.9810	0.921	6.116
14	36	1	0	0.0495	0.099	0.8596	0.841	2.164	0.7738	0.760	1.783
14	36	2	1	0.0495	0.099	0.8548	0.830	2.901	0.8062	0.782	3.001
14	36	1	1	0.0495	0.099	0.8522	0.827	2.957	0.8282	0.799	3.526
14	36	1	2	0.0495	0.099	0.8496	0.826	2.778	0.8566	0.803	6.257
14	36	0	1	0.0495	0.099	0.8440	0.817	3.200	0.9486	0.893	5.861

Table 5

Moisture flux rates under different designed operating conditions, comparison of numerical and experimental results

Designed operating conditions						Comparisons		
$T_{sol,in}$ (℃)	$C_{sol,in}$ (%)	X_{LiCl}	X_{CaCl2}	m_{air} (kg/s)	m_{sol} (kg/s)	MFR	MFR_{exp}	Error (%)
16	24	1	1	0.0495	0.099	0.00396	0.0037	6.575
16	30	1	1	0.0495	0.099	0.00485	0.0041	15.510
16	36	1	1	0.0495	0.099	0.00571	0.0053	7.209
16	42	1	1	0.0495	0.099	0.00640	0.0058	9.425
12	36	1	1	0.0495	0.099	0.00609	0.0054	11.393
14	36	1	1	0.0495	0.099	0.00591	0.0056	5.288
16	36	1	1	0.0495	0.099	0.00571	0.0053	7.209
18	36	1	1	0.0495	0.099	0.00549	0.0048	12.570
16	36	1	0	0.0495	0.099	0.00573	0.00572	0.175
16	36	2	1	0.0495	0.099	0.00572	0.0057	3.197
16	36	1	1	0.0495	0.099	0.00571	0.00569	3.809
16	36	1	2	0.0495	0.099	0.00570	0.00566	7.886
16	36	0	1	0.0495	0.099	0.00569	0.00565	7.150

7. Results and discussion

7.1. Specific humidity of the mixed desiccant solution

Instead of the surface vapour pressure, the equilibrium specific humidity of the mixed solution is adopted to evaluate solution capability to absorb vapour since it is more straight-forward. Based on Eqs. (1) - (10), the specific humidity of the mixed desiccant solution is related to its temperature, concentration and solute mixing ratio. The mixed solutions with concentration of 15%, 30% and 42% are used in this study, and five different mass fraction ratios between LiCl and $CaCl_2$ are adopted: 1:0 (pure LiCl solution), 2:1, 1:1, 1:2 and 0:1(pure $CaCl_2$ solution) for each concentration. The variations of the solution specific humidity with temperature for different mixing ratios under the three concentrations are plotted in Figs. 4-6.

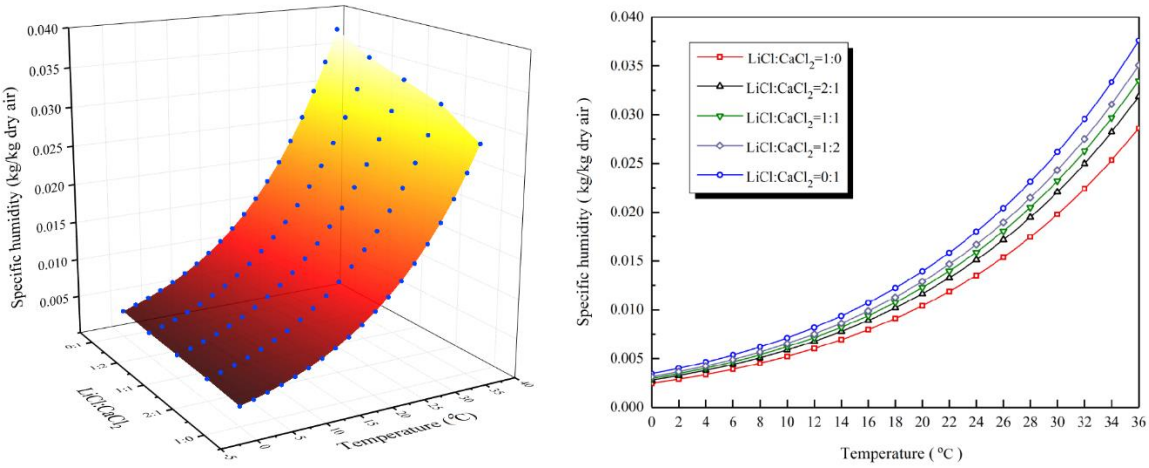

Fig. 4. Mixed solution specific humidity variations with temperature for different mixing ratios under $C_{sol} = 15\%$

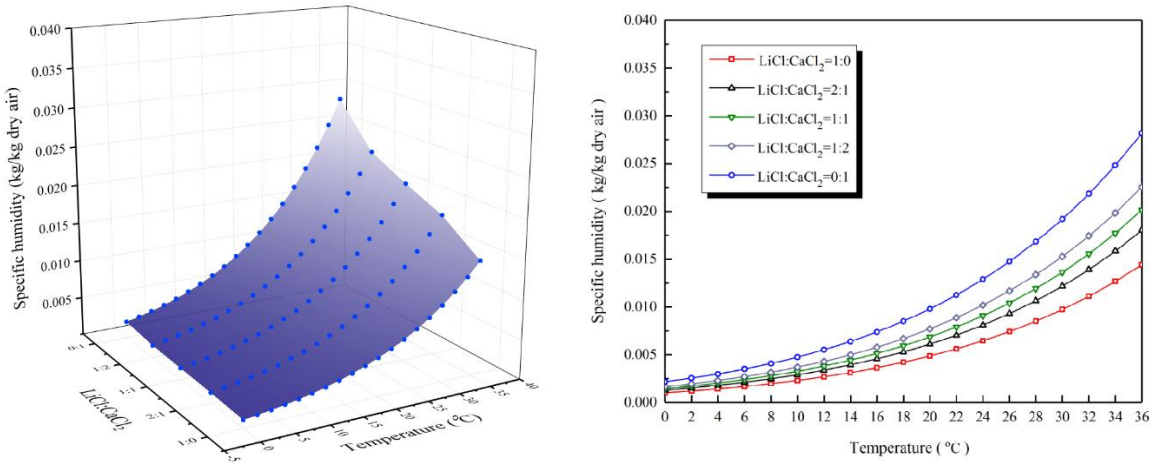

Fig. 5. Mixed solution specific humidity variations with temperature for different mixing ratios under $C_{sol} = 30\%$

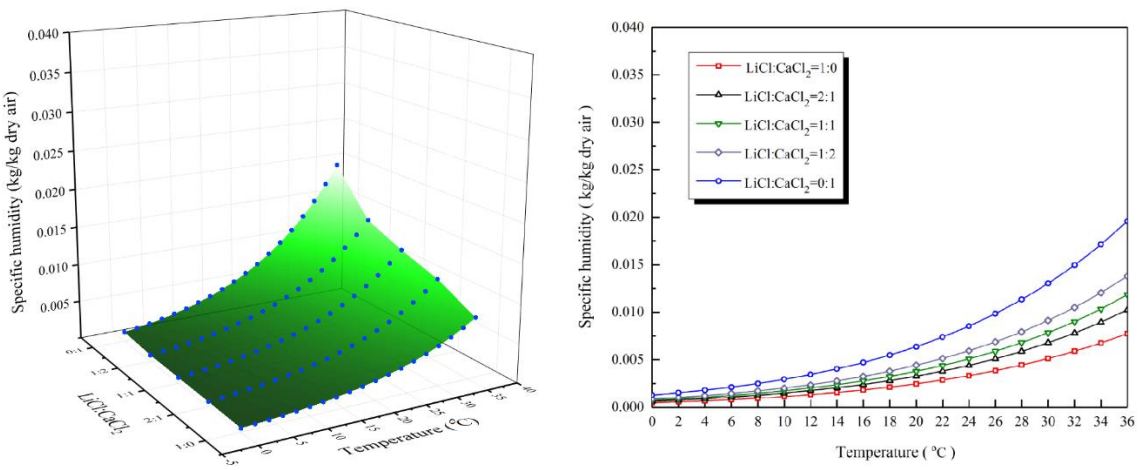

Fig. 6. Mixed solution specific humidity variations with temperature for different mixing ratios under $C_{sol} = 42\%$

As shown in these figures, the mixed solution specific humidity increases with its temperature. For the solution with the low concentration, its temperature influence is larger than that with the high concentration. For example, under $C_{sol} = 15\%$, the specific humidity of the 1:1 mixed solution is increased by 0.03051 (from 0.00297 to 0.03348) kg/kg when its temperature rises from 0℃ to 36℃. By contrast, it is increased by 0.0111 (from 0.00073 to 0.01183) kg/kg under $C_{sol} = 42\%$. In contrast, increasing the solution concentration can enhance the dehumidification ability as well by reducing the solution specific humidity. Taking the 1:1 mixed solution as an example, its maximum specific humidity under C_{sol} of 15%, 30% and 42% are 0.0335, 0.0202 and 0.0118 kg/kg respectively. Apart from T_{sol} and C_{sol}, the mixing ratio is another important parameter influencing the solution specific humidity, which is the main focus of this paper. According to Figs. 4-6, the solution specific humidity decreases with LiCl mass fraction at the given concentration and temperature, this is because pure $CaCl_2$ solution always has the higher specific humidity compared with pure LiCl solution. It is noticed that the influences of the solution temperature, concentration and mixing ratio are interacted with each other. Under the same concentration, the impact of the mixing ratio is insignificant when the solution temperature is relatively low. For example, under $C_{sol} = 42\%$, the specific humidity difference between LiCl and $CaCl_2$ solutions at 36℃ is 0.01185 kg/kg, while the difference is only 0.00213 kg/kg at 12℃. Furthermore, the influence of the mixing ratio increases with the solution concentration, which is illustrated in Fig. 7. It can be seen that the specific humidity difference between LiCl and $CaCl_2$ solutions under 15% is much smaller than that under 42%, meaning the mixing ratio has more significant influence on the solution specific humidity under the high concentration. The solution with high concentration is preferred in dehumidification, increasing LiCl mass fraction leads to the significant performance improvement.

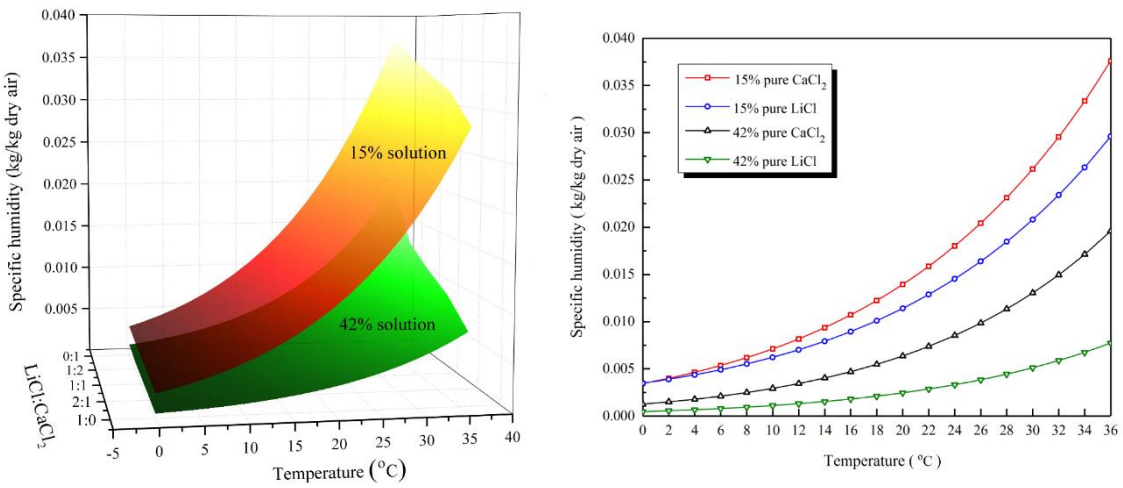

Fig. 7. Mixed solution specific humidity variations for pure LiCl and $CaCl_2$ solutions under different concentrations

7.2. Impact of the mixed solution property on cooling effect

To cool the supply air in the dehumidifier is of vital importance [28-31] since the air with low temperature can save energy used for the subsequent cooling. The cooling effect is evaluated by the sensible effectiveness introduced in Section 4.1. The variations of the sensible effectiveness with the mixing ratio under various solution concentrations and temperatures are given in Figs. 8 and 9.

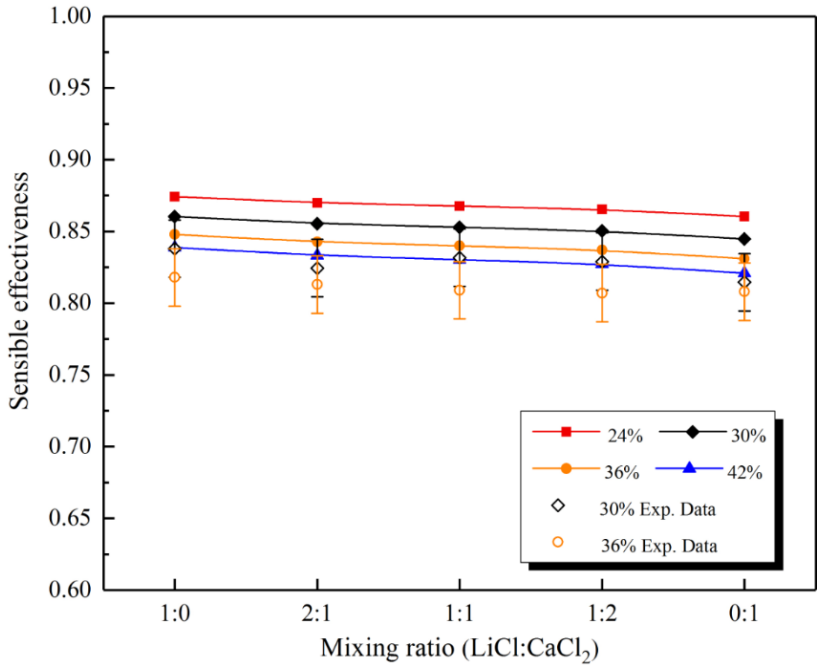

Fig. 8. Sensible effectiveness changes with the mixing ratio under different solution concentrations

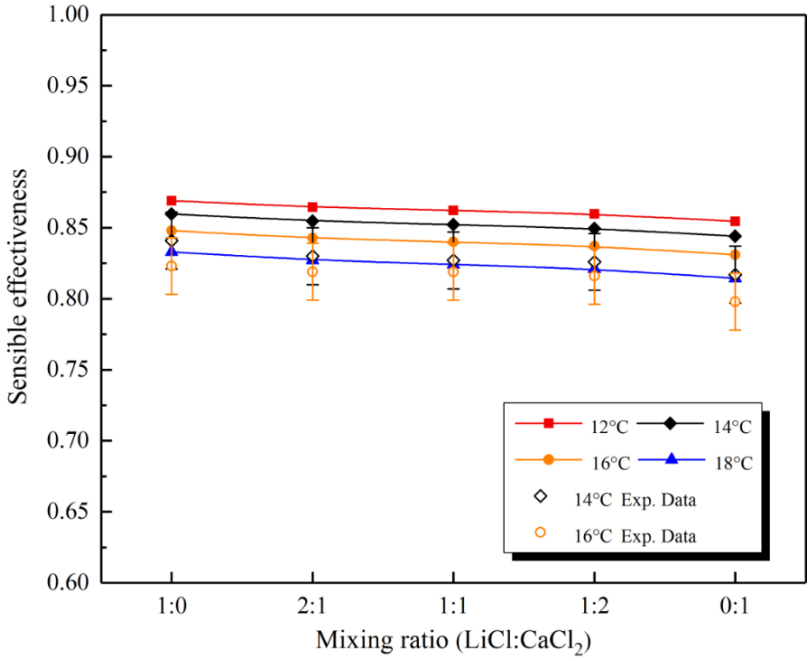

Fig. 9. Sensible effectiveness changes with the mixing ratio under different solution temperatures

It is noticed from these two figures that the sensible effectiveness increases with LiCl mass fraction in the mixed solution, but very weakly. For instance, for the 42% concentration solution, its sensible effectiveness only increases by 2.18% (from 0.8209 to 0.8388) when the mixing ratio ($LiCl:CaCl_2$) changes from 0:1 to 1:0. Similarly, at the solution temperature of 18℃, the sensible effectiveness also increases by 2.28% (from 0.8144 to 0.833) when the mixing ratio changes from 0:1 to 1:0. The dehumidification capacity increases with LiCl mass fraction as well, meaning more latent heat is released. However the sensible effectiveness increases slight rather than being deteriorated. A reasonable explanation for this is given as follows. The air temperature change is induced by two parts: sensible temperature decrease and temperature increase caused by the released latent heat. It can be expressed by:

$$\Delta T = \Delta T_{sen} - \Delta T_{lat} \tag{47}$$

Where ΔT is temperature change of the air; ΔT_{sen} is sensible temperature decrease caused by the temperature difference between the solution and air; ΔT_{lat} is temperature increase caused by the latent heat during dehumidification. It can be further derived as:

$$\Delta T = \Delta T_{sen} - \frac{Q_{lat}}{c_{p,sol}\dot{m}_{sol}} \tag{48}$$

Where Q_{lat} is latent heat released (kW), and it increases with LiCl mass fraction. However, in the meanwhile $c_{p,sol}$ is increased as well. As a result, $\frac{Q_{lat}}{c_{p,sol}\dot{m}_{sol}}$ is slightly decreased due to this combined effect and ΔT is enhanced. Then based on the definition of the sensible effectiveness, it is increased to a small extent.

The influence of the solution concentration on the sensible effectiveness is reflected in Fig. 8. Under the same mixing ratio, increasing the solution concentration leads to the sensible effectiveness decrease. The sensible effectiveness at $C_{sol} = 24\%$ is the highest, while it is the lowest at $C_{sol} = 42\%$. As explained in the previous section, the higher solution concentration, the lower solution specific humidity. Thus the latent heat released during the dehumidification is increased, the cooling effect is reduced based on Eq. (48). With regard to the solution temperature, it has negative effect on the sensible effectiveness as well, as displayed in Fig. 9. The highest sensible effectiveness is at 12℃, while it reaches the lowest at 18℃. This is easy to understand since increasing the solution temperature will significantly reduce the temperature difference between the solution and air, the heat transfer potential is decreased as well. This leads to the sensible effectiveness decrease.

7.3. Impact of the mixed solution property on dehumidification effect

Dehumidification is the key function of the heat and mass exchanger. Similar to cooling effect, the dehumidification effect is also closely related to the solution properties: concentration, temperature and mixing ratio. The influences of the solution mixing ratio on the latent effectiveness under various concentrations are plotted in Fig. 10.

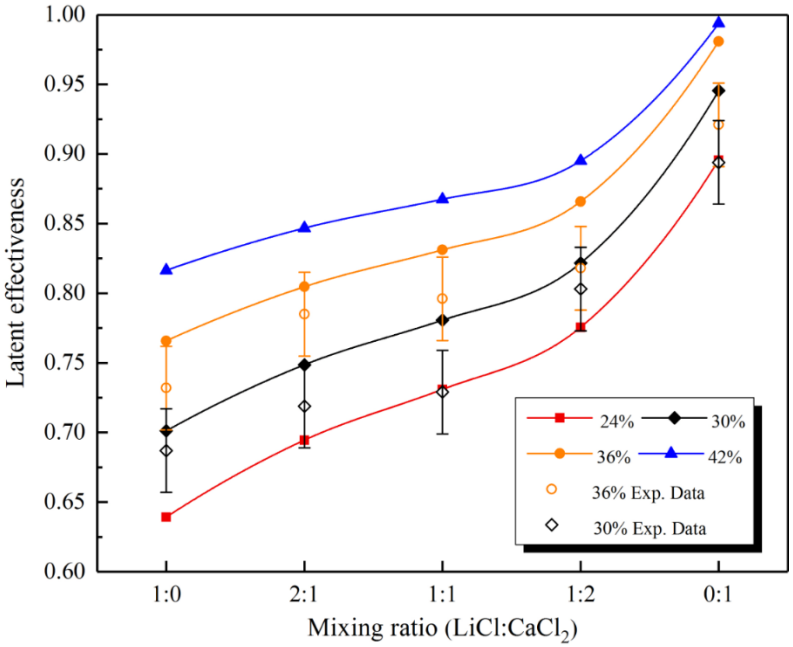

Fig. 10. Latent effectiveness changes with mixing ratio for different solution concentrations

Firstly, the impact of the solution concentration on the latent effectiveness is explored. As clearly illustrated in Fig. 10, the higher solution concentration, the better the system dehumidification effect. For example, for the solution with a mixing ratio of 1:1, its latent effectiveness increases by 18.69% (from 0.7309 to 0.8675) when C_{sol} changes from 24% to 42%. For the 2:1 mixed solution, its latent effectiveness increases by 21.94% (from 0.6945 to 0.8467) when C_{sol} varies from 24% to 42%, and the similar cases are found for the other mixing

ratios. This can be reflected by the variations of the moisture flux rate (MFR) and air outlet specific humidity ($W_{air,out}$) with the solution concentration as well.

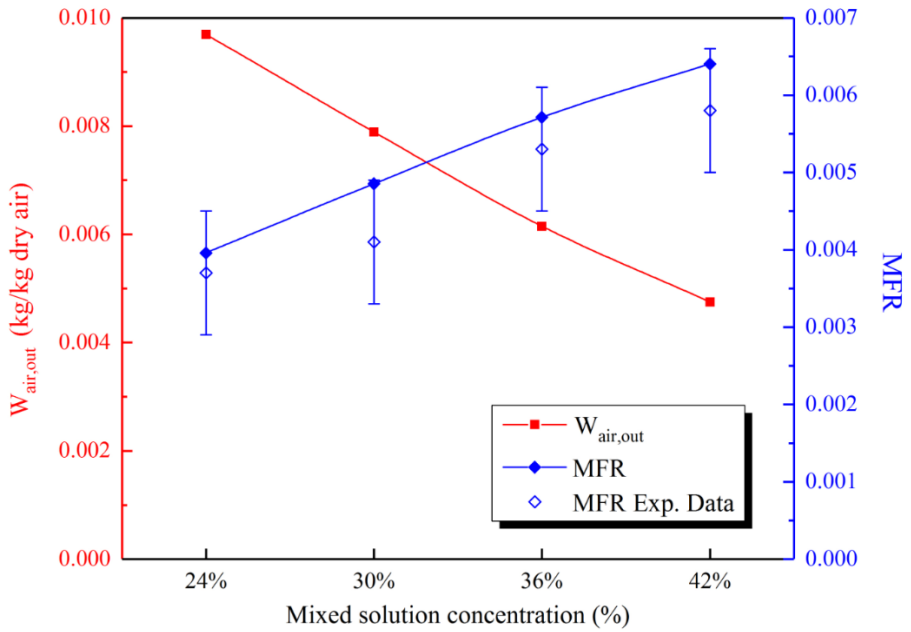

Fig. 11. Impact of solution concentration on MFR and $W_{air,out}$

The effects of the solution concentration on the MFR and $W_{air,out}$ are shown in Fig. 11 for a mixing ratio of 1:1. It can been seen from this figure that the MFR increases by 61.7% (from 0.00396 to 0.0064) when the solution concentration varies from 24% to 42%. In the meanwhile $W_{air,out}$ reduces from 0.00969 $kg/kg\ dry\ air$ to 0.00475 $kg/kg\ dry\ air$, meaning the dehumidification effect is considerably improved. This can be explained by the variation of the solution specific humidity with its concentration. As mentioned previously, the solution specific humidity decreases with its concentration. Therefore, the mass transfer potential between the solution and air is improved, so the MFR increases. As for the latent effectiveness, based on its definition given in Eq. (37), although the solution inlet specific humidity is decreased, the significant rise of the humidity difference between the inlet and outlet air still improves the latent effectiveness. As shown in Fig. 10, the influence of the solution concentration becomes weak with $CaCl_2$ mass fraction in the mixed solution. For example, for pure LiCl solution, the latent effectiveness can be improved by 27.7% (from 0.6393 to 0.8164) when the solution concentration varies from 24% to 42%. By contrast, for pure $CaCl_2$ solution, it is increased by 10.98% only (from 0.8955 to 0.9938).

Apart from the solution concentration, its temperature should be taken into consideration as well since it is closely related to the mixed solution surface vapour pressure. The changes of the latent effectiveness with the mixing ratio under different solution temperatures are plotted in Fig. 12, while the variations of the MFR and $W_{air,out}$ with the solution temperature are shown in Fig. 13.

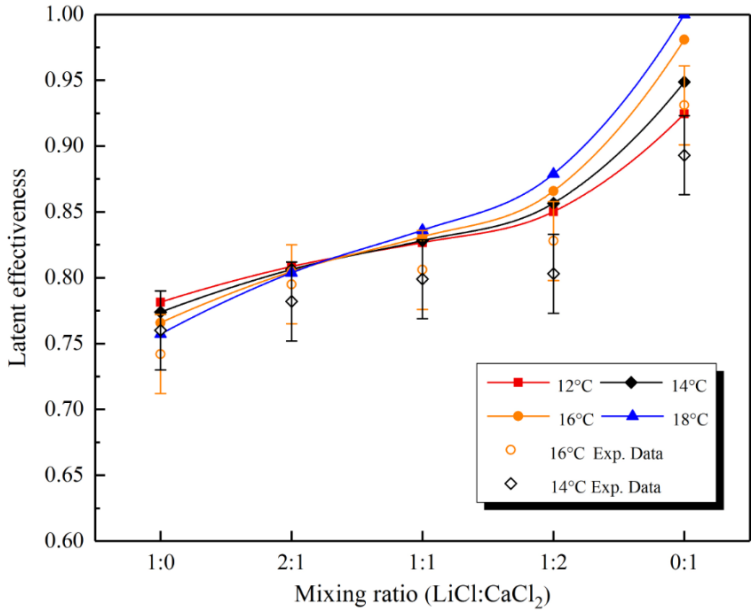

Fig. 12. Latent effectiveness changes with mixing ratio for different solution temperatures

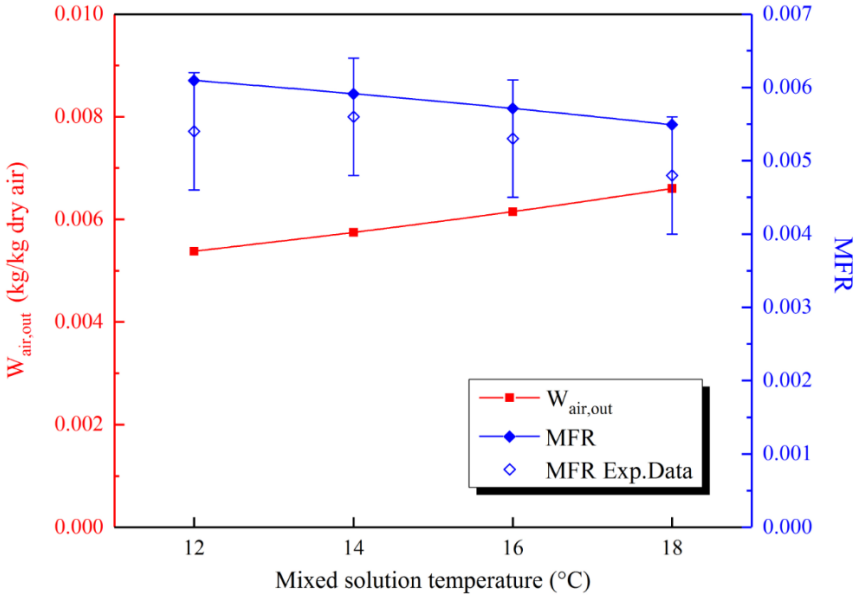

Fig. 13. Impacts of solution temperature on MFR and $W_{air,out}$

As indicated in Fig. 12, the solution temperature has different effects on the latent effectiveness under different mixing ratios. For the LiCl:$CaCl_2$=1:0 solution, the latent effectiveness is high at low temperature. For the LiCl:$CaCl_2$=1:2 and 0:1 solutions, increasing the solution temperature can improve the latent effectiveness. For the LiCl:$CaCl_2$=2:1 and 1:1 solutions, the influence of the solution temperature on the latent effectiveness is negligible. For example, for the LiCl:$CaCl_2$=2:1 solution, the maximum difference of the latent effectiveness at the measured temperature range is only 0.0048 (the maximum value is 0.8085 at $T_{sol} = 12℃$ while the minimum value is 0.8037 at $T_{sol} = 18℃$). As explained previously, the lower solution temperature, the lower solution specific humidity, thus the mass transfer potential between the

solution and air is increased. In the meanwhile, the solution inlet specific humidity is decreased, so the air humidity difference between the air at outlet and inlet is increased and the system dehumidification ability is improved. With referring to Eq. (37), both the numerator and denominator are increased, this combined effect would lead to different influences on the latent effectiveness. However, if only the amount of moisture being absorbed in the dehumidifier is considered, the system will benefit greatly from decreasing the solution temperature. This is reflected in Fig. 13 as well, where the MFR and $W_{air,out}$ variations with the solution temperature for the solution with the mixing ratio of 1:1 are plotted. As can be seen from Fig. 13 that the MFR is raised by 11% (from 0.00549 to 0.00609), and the $W_{air,out}$ is decreased by 18.52% (from 0.006598 to 0.005376 $kg/kg\ dry\ air$) when the solution temperature reduces from 18℃ to 12℃.

Finally the influence of the mixing ratio on the dehumidification effect is investigated. For a better understanding of the mixing ratio effect, the MFR and $W_{air,out}$ variations with the mixing ratio are plotted in Fig. 14.

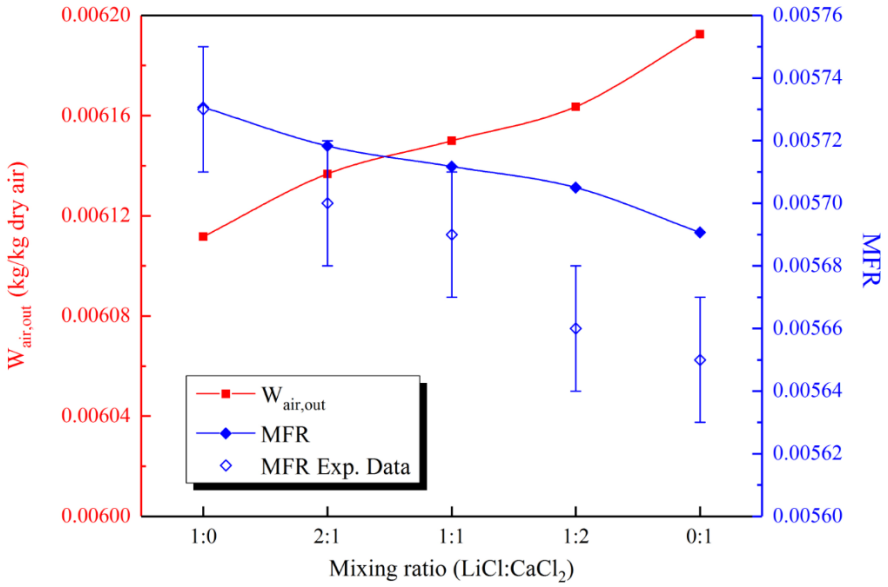

Fig. 14. Influences of solution mixing ratio on MFR and $W_{air,out}$

LiCl has been proved to have better moisture absorbing ability compared with $CaCl_2$, and this is in accordance with the results shown in Fig. 14. In this figure, the mixed solution concentration and temperature are maintained at 36% and 16℃ respectively. When $CaCl_2$ mass fraction increases from 0 to 1, the MFR is reduced from 0.00573 to 0.00569, while the $W_{air,out}$ is increased from 0.00611 to 0.0062 $kg/kg\ \ dry\ air$. This is because the specific humidity ratio of pure $CaCl_2$ solution is always higher than that of pure LiCl solution under the same concentration and temperature. However, it should be pointed out that the mixing ratio has less impact on the dehumidification ability compared with the solution concentration and temperature. In Figs. 11 and 13, the MFR can be improved by 61.7% and 11% respectively by

increasing concentration from 24% to 42%, or reducing temperature from 18℃ to 12℃. By contrast it is only improved by 1.63% by increasing LiCl mass fraction from 0 to1. With regard to the latent effectiveness, both Fig. 10 and Fig. 12 reveal that the latent effectiveness increases with CaCl2 mass fraction. According to Eq. (37), the numerator would be decreased with $CaCl_2$ mass fraction, so less moisture is absorbed. However the solution inlet specific humidity $W_{sol,in}$ is increased as well, which leads to the decrease of the denominator. This offsetting effect finally improves the latent effectiveness.

7.4. Impact of the solution mixing ratio on system COP

The previous sections are about impact of the main solution properties on the cooling and dehumidification effects. In this section, the system energy efficiency is evaluated by applying the COP analysis. According to Eq. (44), the COP is closely related to the system sensible and latent cooling outputs, and the heat input for regeneration. First of all, the regeneration heat input Q_{reg} is assessed.

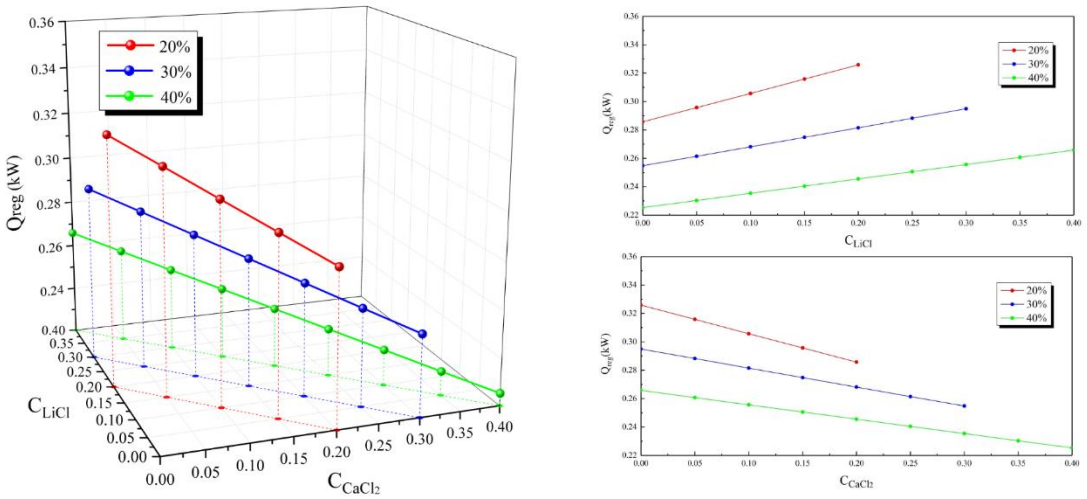

Fig. 15. Variations of Q_{reg} with contents of LiCl and $CaCl_2$ at 16℃

The relationship between Q_{reg} and the solute content at the mixed solution temperature $T_{sol,in} = 16$℃ is reflected in Fig. 15. It is noticed that when the mixed solution concentration increases, Q_{reg} tends to decline. For instance, Q_{reg} varies from 0.286 to 0.326 kW for the 20% solution when LiCl mass fraction changes from 0 to 0.4, while it varies from 0.255 to 0.295 kW for the 30% solution, and from 0.225 to 0.266 kW for the 40% solution respectively. The system dehumidification effect is improved by applying the high concentration solution, as a result more latent heat is released during this process, the solution outlet temperature is increased. For example, $T_{sol,out}$ for the 1:1 mixed solution at 20% concentration is 21.84℃, while it is 23.11℃ at 30% concentration and 24.31℃ at 40% concentration. Then based on Eq. (47), the temperature difference between $T_{sol,out}$ and T_{reg} is narrowed, meaning the less

energy is required for regeneration. With referring to the influence of the solute content again, as shown in Fig. 15, Q_{reg} reduces significantly with $CaCl_2$ mass fraction in the mixed solution. This seems to be inconsistent with the impact of the solution concentration, as increasing $CaCl_2$ can reduce the latent heat transfer, which reduces $T_{sol,out}$. However, it should also be noted that when $CaCl_2$ mass fraction is increased, the air cooling effect is reduced, thus $T_{air,out}$ will be increased. This combined effect leads to the rise of $T_{sol,out}$. Taking the 40% solution as an example, $T_{sol,out}$ increases gradually from 24.03 to 24.76 ℃ when C_{CaCl_2} varies from 0 to 0.4. So the heat input for regeneration is reduced.

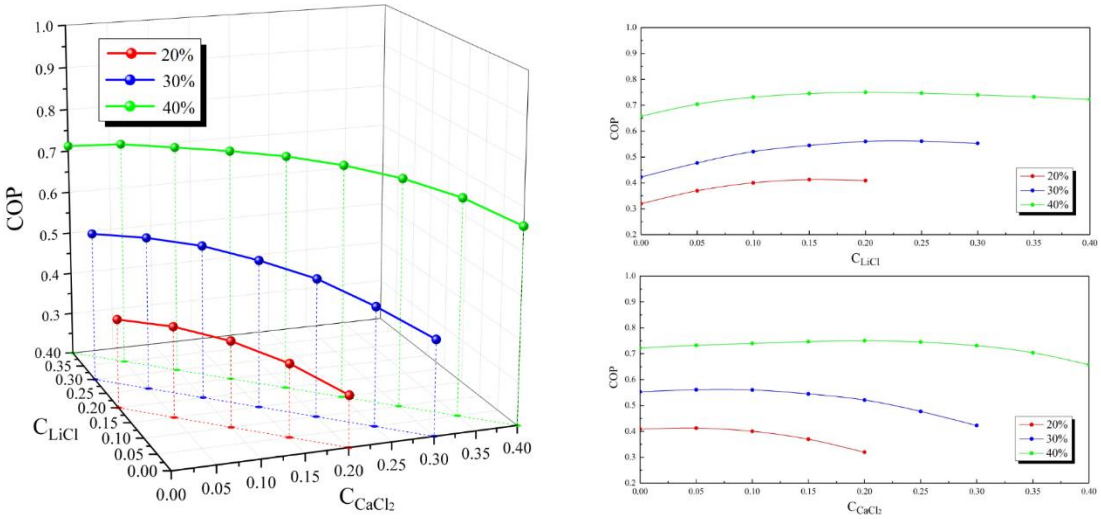

Fig. 16. Variations of COP with contents of LiCl and $CaCl_2$ at 16℃

Afterwards the relationships between the COP and solute content are plotted in Fig. 16. Obviously the COP differences among various mass fractions are dramatic, and can be significantly increased by raising the solution concentration. The maximum COPs for the 20%, 30% and 40% solutions are 0.413, 0.56 and 0.749 respectively. The sensible heat output is decreased slightly with the solution concentration, this is due to more heat released during the dehumidification. The latent heat output is increased due to the better dehumidification effect, and Q_{reg} is reduced as discussed previously. So the dramatic difference of the COP between different concentrations is easily understood.

Then the influences of the solute contents on the system COP are explored. As discussed in Sections 7.2 and 7.3, increasing $CaCl_2$ mass fraction will reduce both the cooling and dehumidification effects due to the increased $T_{air,out}$ and reduced MFR. This is reflected in Fig. 17 where $T_{air,out}$ increases from 17.95℃ to 18.57℃, and the MFR decreases from 0.0082 to 0.0063 when $CaCl_2$ mass fraction changes from 0 to 0.3. As a result, both Q_{sen} and Q_{lat} are reduced. In the meanwhile Q_{reg} is reduced as well due to the increased solution outlet

temperature. This is also illustrated in Fig. 17 that $T_{sol,out}$ increases from 22.83℃ to 23.61℃ when $CaCl_2$ mass fraction changes from 0 to 0.3.

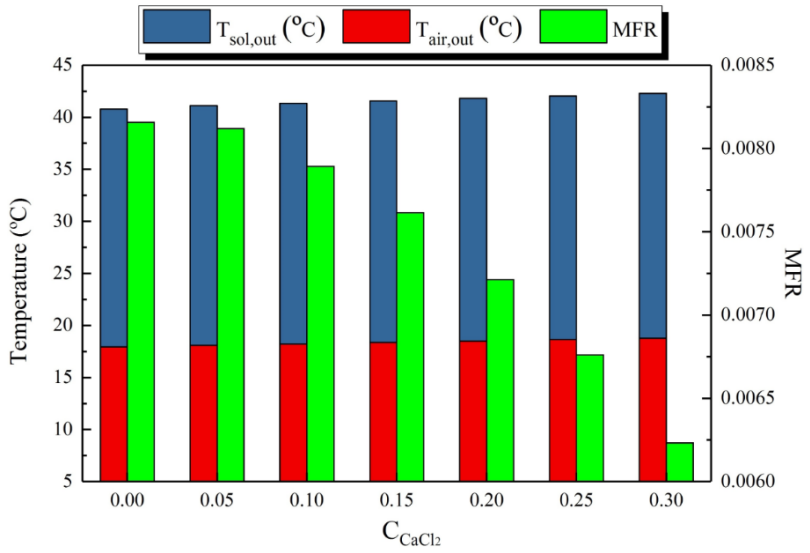

Fig. 17. Variations of $T_{sol,out}$, $T_{air,out}$ and MFR with $CaCl_2$ mass fraction

The variations of the total cooling output (the sum of the sensible and latent cooling output) and Q_{reg} with $CaCl_2$ mass fraction for the 30% solution are shown in Fig. 18. It can be noticed that the total cooling output decreases from 0.163 to 0.108 kW as $CaCl_2$ mass fraction rises from 0 to 0.3, while Q_{reg} decreases from 0.294 to 0.255 kW. As a result, the system COP initially increases with $CaCl_2$ mass fraction, then drops off afterwards.

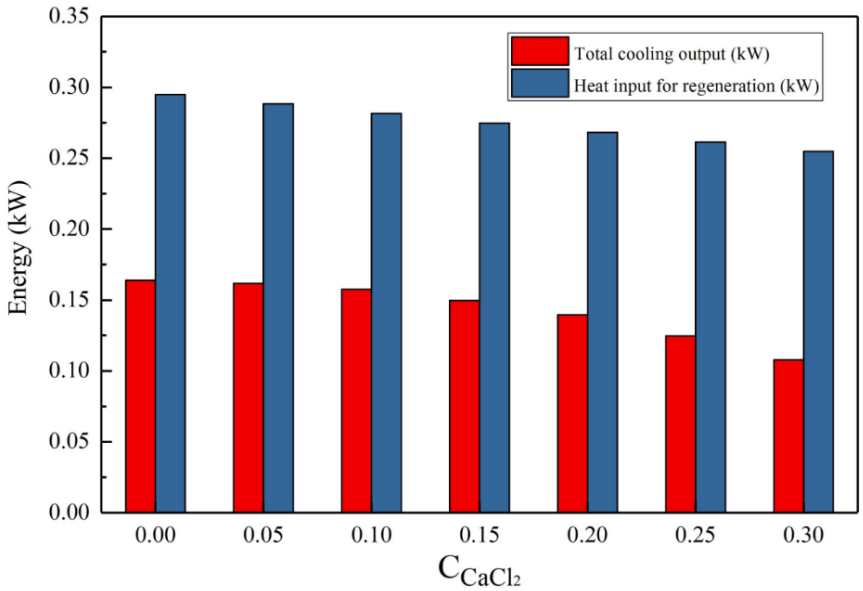

Fig. 18. Variations of total cooling output and Q_{reg} with $CaCl_2$ mass fraction for 30% desiccant solution

Compared with pure LiCl solution, the system COP can be improved by adopting the mixed solution. For the 20%, 30% and 40% solutions, the system COPs can be increased by 28.13%, 30.23% and 15.38% respectively compared with pure LiCl solution. For the 20% solution, the system COP peaks at 0.413 when LiCl:$CaCl_2$=3:1. But for the 30% solution, the COP peaks at 0.56 when LiCl:$CaCl_2$=2:1, while for the 40% solution, its COP peaks at 0.749 when LiCl:$CaCl_2$=1:1. Thus under different solution concentrations, the optimum mixing ratio for the highest COP is different, and the higher the solution concentration, the more $CaCl_2$ shall be added. This is useful for selecting the optimum mixing ratio under different concentrations. Currently the LiCl price in the UK is 40£/kg, while the $CaCl_2$ price is only 1.5£/kg. Considering the price difference between LiCl and $CaCl_2$, applying the mixed solution can not only increase the system efficiency but also save material cost as well.

8. Conclusions

The effects of the mixed LiCl-$CaCl_2$ desiccant properties on the performance of a membrane-based dehumidification system are analysed in this paper. The finite difference method is used to develop the governing equations in the numerical simulation, and the NRTL method is applied for the mixed solution property calculation. The experimental tests are carried out to validate the numerical modelling. The optimum mixing ratio is identified based on the system COP analysis. The main conclusions are given as follows:

- The specific humidity of the mixed solution can be reduced by decreasing its temperature, increasing its concentration, and applying the solution with high LiCl content.
- The effects of the solution temperature, concentration and mixing ratio interact with each other. Under the same concentration, the mixing ratio influence is insignificant when the solution temperature is relatively low. The mixing ratio has more significant effect at the high concentration.
- The system cooling performance can be enhanced by applying the mixed solution with low concentration, temperature and $CaCl_2$ content, while its dehumidification capacity can be increased by using the strong and cool solution. Increasing LiCl content can improve the dehumidification effect, but its influence is relatively weak compared with the solution concentration and temperature effects.
- The regeneration heat Q_{reg} can be dramatically saved, and the high system COP can be achieved by increasing either the solution concentration or $CaCl_2$ content.
- Compared with the pure LiCl solution system, the mixed solution system COP can be raised up to 30.23% by increasing $CaCl_2$ content at a 30% solution concentration. The system COP initially increases with $CaCl_2$ content, then drops off.

- The optimum mixing ratio varies with the solution concentration. For the LiCl-$CaCl_2$ solution, the highest COPs appear at the mixing ratios of 3:1, 2:1 and 1:1 for 20%, 30% and 40% concentrations respectively. More $CaCl_2$ shall be added to the high concentration solution for achieving the better performance.

Acknowledgements

This research was supported by the International Exchanges 2015 Cost share Programme of the Royal Society (Grant No. IE150678).

References

[1] Yun GY. Influences of perceived control on thermal comfort and energy use in buildings, Energy and Buildings. 2018; 158:822-830.

[2] Wu BJ, Cai WJ, Ji K. Heat source effects on thermal comfort for active chilled beam systems, Building and Environment. 2018; 141:91-102.

[3] Xu Y, Zhang YP. An improved mass transfer based model for analysing VOC emissions from building materials, Atmospheric Environment. 2003; 37:2497-2505.

[4] Perez-Lombard L, Ortiz J, Pout C. A review on buildings energy consumption information, Energy and Buildings. 2008; 40:394–398.

[5] The CIBSE Journal CPD Programme: liquid desiccant for dehumidification in building air conditioning systems.

[6] Afroz Z, Shafiullah GM, Urmee T, Higgins G. Modeling techniques used in building HVAC control systems: A review, Renewable and Sustainable Energy Reviews. 2018; 83:64-84.

[7] Zhang J, Zhu N, Wu Y. The analysis of energy consumption of a commercial building in Tianjin, China, Energy Policy. 2009; 37:2092-7.

[8] Ge GM, Xiao F, Niu XF. Control strategies for a liquid desiccant air-conditioning system, Energy and Buildings. 2011; 43:1499-1507.

[9] Ramzy A, ElAwady WM, Abdel Meguid H. Modeling of heat and moisture transfer in desiccant packed bed utilizing spherical particles of clay impregnated with $CaCl_2$, Applied Thermal Engineering. 2014; 66:499-506.

[10] Liu XH, Geng KC, Lin BR, Jiang Y. Combined cogeneration and liquid desiccant system applied in a demonstration building, Energy and Buildings. 2004; 36:945-953.

[11] Dai YJ, Wang RZ, Zhang HF, Yu JD. Use of liquid cooling to improve the performance of vapor compression air conditioning, Applied Thermal Engineering. 2001; 21:1185-1202.

[12] Huang SM, Zhang LZ. Researches and trends in membrane-based liquid air dehumidification, Renewable and Sustainable Energy Reviews. 2013; 28:425-440.

[13] Liu XH, Jiang Y, Yi XQ. Effect of regeneration mode on the performance of liquid desiccant packed bed regenerator, Renewable Energy. 2009; 34(1):209-16.

[14] Zhang LZ. Progress on heat and moisture recovery with membranes: from fundamentals to engineering applications, Energy Conservation and Management. 2012; 63:173-95.

[15] Zhang LZ. Heat and mass transfer in a cross-flow membrane-based enthalpy exchanger under naturally formed boundary conditions, International Journal of Heat and Mass Transfer. 2007; 50:151-162.

[16] Zhang LZ, Liang CH, Pei LX. Conjugate heat and mass transfer in membrane-formed channels in all entry regions, International Journal of Heat and Mass Transfer. 2010; 53:815-824.

[17] Huang SM, Zhang LZ, Tang K, Pei LX. Fluid flow and heat mass transfer in membrane parallel-plates channels used for liquid desiccant air dehumidification. International Journal of Heat and Mass Transfer 2012; 55:2571-2580.

[18] Huang SM, Zhang LZ, Yang ML. Conjugate heat and mass transfer in membrane parallel-plates ducts for liquid desiccant air dehumidification: Effects of the developing entrances. Journal of Membrane Science 2013; 437:82-89.

[19] Moghaddam DG, Oghabi A, Ge GM, Besant RW, Simonson CJ. Numerical model of a small-scale liquid-to-air membrane energy exchanger: Parametric study of membrane resistance and air side convective heat transfer coefficient, Applied Thermal Engineering. 2013; 61; 245-258.

[20] Moghaddam DG, Le Poudre P, Besant RW, Simonson CJ. Steady-state performance of a small-scale liquid-to-air membrane energy exchanger for different heat and mass transfer directions, and liquid desiccant types and concentrations: experimental and numerical data, ASMEJ Heat Transfer. 2013; 135:1–13.

[21] Moghaddam DG, LePoudre P, Ge GM et al. Small-scale single-panel liquid-to-air membrane energy exchanger (LAMEE) test facility development, commissioning and evaluating the steay-state performance, Energy and Buildings. 2013; 66:424-436.

[22] Vali A, Ge GM, Besant RW, Simonson CJ. Numerical modelling of fluid flow and coupled heat and mass transfer in a counter-cross-flow parallel-plate liquid-to-air membrane energy exchanger, Int J Heat Mass Transfer. 2015; 89:1258-1276.

[23] Moghaddam DG, Besant RW, Simonson CJ. Solution-side effectiveness for a liquid-to-air membrane energy exchanger used as a dehumidifier/regenerator, Applied Energy. 2014; 113:872-882.

[24] Bai HY, Zhu J, Chen ZW, Ma LN, Wang RZ, Li TX, Performance testing of a cross-flow membrane-based liquid desiccant dehumidification system, Applied Thermal Engineering, 2017; 119:119-131.

[25] Bai HY, Zhu J, Chen ZW, Chu JZ. Parametric analysis of a cross-flow membrane-based parallel-plate liquid desiccant dehumidification system: numerical and experimental data, Energy and Buildings, 2018; 158:494-508.

[26] Dong C, Lu T, Wen T. Experimental study on dehumidification performance enhancement by TiO_2 superhydrophilic coating for liquid desiccant plate dehumidifiers, Building and Environment, 2017; 124:219-231.

[27] Liu J, Liu X, Zhang T. Performance comparison of three typical types of internally-cooled liquid desiccant dehumidifiers, Building and Environment. 2016; 103:134-145.

[28] Qiu D, Wu ZH, Huang SM, Ye WB, Chen XL, Luo JC, Yang ML. Laminar flow and heat transfer in and internally-cooled hexagonal parallel-plate membrane channel (IHPMC), Applied Thermal Engineering. 2017; 124:767-780.

[29] Huang SM, Qiu D, Huang WH, Yang ML, Xiao HM. Laminar flow and heat transfer in a quasi-counter flow parallel-plate membrane channel in the solution side with cooling tubes, International Journal of Heat Mass Transfer. 2017; 105:769-780.

[30] Huang SM, Yang ML, Hu B, Tao S, Qin FGF, Weng WL, Wang WH, Liu J. Performance analysis of an internally-cooled plate membrane liquid desiccant dehumidifier (IMLDD): An analytical solution approach, International Journal of Heat and Mass Transfer. 2018; 119:577-585.

[31] Huang SM, Yang ML, Hong YX, Ye WB. Performance correlations of an adjacently internally-cooled membrane contractor applied for liquid desiccant air dehumidification, Applied Thermal Engineering. 2018; 129:1660-1669.

[32] Lin J, Huang SM, Wang RZ, Chua KJ. Thermodynamic analysis of a hybrid membrane liquid desiccant dehumidification and dew point evaporative cooling system, Energy Conversion and Management. 2018; 156:440-458.

[33] Zhao X, Li XW, Zhang XS. Selection of optimal mixed liquid desiccants and performance analysis of the liquid desiccant cooling system, Applied Thermal Engineering. 2016; 94:622-634.

[34] Ertas A, Anderson EE, Kiris I. Properties of a new liquid desiccant solution-lithium chloride and calcium chloride mixture, Solar Energy. 1992; 49(3):205-212.

[35] Ahmed SY, Gandhidasan P, AI-Farayedhi AA. Thermodynamic analysis of liquid desiccants, Solar Energy. 1998; 62:11-18.

[36] Nilson LE. Predicting the properties of mixtures, 1978, Mixing Rules in Science and Engineering. Marcel Dekker, New York.

[37] Chen CC, Evans LB. A local composition model for the excess Gibbs energy of aqueous electrolyte systems, AIChE. 1986; 32(3):444-454.

[38] Chen CC, Britt HI, Boston JF, Evans LB. Local composition model for excess Gibbs energy of electrolyte systems. Part a: Single solvent, single completely dissociated electrolyte systems, AIChE. 1982; 28(4):588-596.

[39] Yao Y, Yu YB, Zhu ZY. Experimental investigations on surface vapor pressure models for LiCl-$CaCl_2$ desiccant solutions, Solar Energy. 2016; 126:1-13.

[40] Zhu ZY, Yao Y. Verification and research on the vapour pressure of mixed LiCl-$CaCl_2$ solution, Journal of Refrigeration. 2015; 36(6):52-56.

[41] Li XW, Zhang XS, Wang G, Cao RQ. Research on ratio selection of a mixed liquid desiccant: Mixed LiCl-$CaCl_2$ solution, Solar Energy. 2008; 82:1161-1171.

[42] Li XW, Zhang XS, Wang F, Zhao X, Zhang Z. Research on ration selection of mixed absorbent solution for membrane air-conditioning system, Energy Conversion and Management. 2015; 89:111-119.

[43] Alduchov OA, Eskridge RE. Improved magnus form approximation of saturation vapour pressure, Journal of applied meteorology. 1996; 35(4):601-9.

[44] ASHRAE, *2013 ASHRAE Handbook Fundamentals.* Atlantal 2013.

[45] Simonson CJ, Besant RW. Energy wheel effectiveness: Part 1 – Development of dimensionless groups, Int J Heat Mass Transfer. 1999; 42:2161-70.

[46] Taylor JR. An Introduction to Error Analysis: The Study of Uncertainties in Physical Measurements, second ed., University Science Books, Sausalito, CA, 1997.

Nomenclature

a_w	activity of water
A	area (m^2)
A_ϕ	Debye-Huckel constant
c_p	specific heat capacity at constant pressure $J/(kgK)$
C	concentration (%)
COP	coefficient of performance
C_r^*	thermal capacity ratio
d	width of the air or solution channel (m)

D	mass diffusivity (m^2/s)
f_w	activity coefficient of water
h	convective heat transfer coefficient $W/(m^2K)$
h_{fg}	water vapour adsorption heat (J/kg)
h^*	operating factor
H	unit height (m)
I_x	ionic strength in mole fraction scale
k	thermal conductivity $W/(mK)$
L	unit length (m)
LRC	long range interaction
MFR	moisture flux rate
MRR	moisture removal rate (kg/s)
M_w	molecular weight of water ($kg/kmole$)
m^*	solution to air mass flow rate ratio
$\dot{m}$	mass flow rate (kg/s)
NRTL	electrolyte non-random two-liquid method
NTU	number of heat transfer units
NTU_m	number of mass transfer units
P	pressure (pa)
P_v	equilibrium surface vapour pressure of liquid desiccant (pa)
Q	energy power (kW)
Re	Reynolds number
SMR	simple mixing rules
SRC	short range interaction
T	temperature (℃)
U	heat transfer coefficient $W/(m^2K)$
U_m	mass transfer coefficient $kg/(m^2s)$
$\dot{V}$	volumetric flow rate (l/min)
W	humidity ratio (kg/kg dry air)
X	mass fraction
x	mole concentration

Greeks

ε	effectiveness
δ	Membrane thickness (m)
ρ	density (kg/m^3)

τ	binary interaction energy parameter
χ	closest approach parameter of the Pitzer-Debye-Huckel equation

Superscripts

$*$	dimensionless

Subscripts

air	air flow
$desi$	desiccant flow
exp	experimental
in	inlet
lat	latent
m	mass transfer
mem	membrane
num	numerical
out	outlet
reg	regeneration
sen	sensible
sol	solution flow
w	water